Experimental investigation of flow pattern over a fully developed bed at a 60° river confluence in large floods

Behnam Balouchi[1] · Mahmood Shafai-Bejestan[2] · Nils Ruther[1] · Mostafa Rahmanshahi[2]

Abstract

River confluences have a complex flow and sedimentation pattern that have vital influences on the hydraulic and bed morphology of river reach and the surrounding area. Confluences can be observed in waterways with various situations such as live bed conditions. This condition is a hydro-morphological situation with a high densimetric Froude number, i.e., bed load transport is supplied from upstream. According to the literature review, most of the experimental studies investigate the flow pattern on the flatbed and not on the developed riverbed, or/and in the low densimetric Froude number, or/and without supplying the sediment from upstream. Therefore, in the present study for the quantification of the flow pattern under these conditions, each developed bed was fixed with the cement blanket method in the laboratory. Then, the 3D velocity was measured at specific points at the confluence. The current study was designed to understand the flow pattern corresponding to the river bed behavior in the case of large floods. It is expected that the morphological features downstream of the confluence have a different pattern than the ones in the condition described in other literature. Thus, this paper describes briefly what are the different bed features and investigates the corresponding flow pattern. The results of the flow pattern on the developed bed show that all zones at the river confluence can be observed except the point bar due to the approximate equality of the mean longitudinal velocity of the separation zone and the main channel upstream of the confluence. Moreover, results show that by increasing the bedload ratio (sediment discharge to water discharge of the main channel of upstream of the confluence) from 0 to 3×10^{-4}, flow deflection to the outer bank of the channel decreased down to 45%, the stagnation equivalent area decreased down to 2.5 times, and bed shear stress decreased down to 40%. Hence, the momentum of lateral flow decreased with increasing bedload. Besides, the recovery zone occurred at a longer distance after the confluence compared to the case without bedload. Hence, the location of the maximum velocity zone, vortices, and secondary flows changed downstream of the confluence, by changing the bed load value.

Keywords River confluence · Developed bed · Live bed · Bedload · Flow pattern · Point bar

Introduction

River confluences are always challenging sections of river networks. Whether man-made or completely unregulated occurring, they are dominated by a complex 3D flow

✉ Behnam Balouchi
  behnamm_1988@yahoo.com

[1] Department of Civil and Environmental Engineering, Norwegian Institute of Science and Technology, Trondheim, Norway

[2] Faculty of Water and Environmental Engineering, Shahid Chamran University of Ahvaz, Ahvaz, Iran

pattern and under constant change. Best (1987) is one of the pioneers who investigated the flow structure in river confluences. He showed six main zones at river confluences (Fig. 1). According to Fig. 1, the stagnation zone is located at the upstream side of the junction point. Flow deflection zone was formed due to combined flows from the main and tributary channels. Zone of separation is located at the downstream side of the junction point and is the main reason for a horizontal vortex in this zone that leads to the sedimentation and generates a point bar. Maximum velocity or flow contraction zone can accelerate erosion on the outer bank and lead to lateral movement of an original river bed. The consequent high flow velocities, shear layer effect, and vortexes in this zone can also make difficulties for navigation (Weber et al. 2001); and the flow recovery zone is
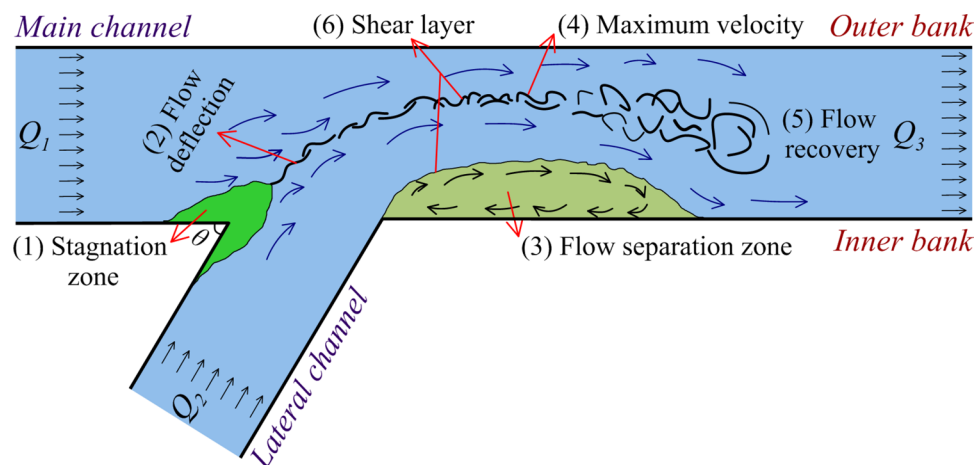
Fig. 1 River confluence zones (adopted from Best 1987)

the location where the influence of confluence on the flow diminishes gradually.

According to the mentioned complexity and importance of river confluences, many studies were attempted in the literature which can divide into three categories based on the focus of the current study. These three categories can be: 1) numerical modeling and/or fieldwork, 2) physical modeling of sediment pattern, and 3) physical modeling of flow pattern. Among the studies that evaluate the flow and sediment patterns of river confluence by numerical modeling and/or fieldwork, one can mention Bradbrook et al. (2001), Boyer et al. (2006), Shakibainia et al. (2010), Constantinescu et al. (2011, 2012), Bahmanpouri et al. (2017), Ahadiyan et al. (2018), Gualtieri et al. (2018), Gualtieri et al. (2019), Balouchi et al. (2021), Bahmanpouri et al. (2022). Besides some studies investigated the effect of geometric and hydraulic conditions on sedimentation pattern such as Ghobadian and Shafai Bejestan (2007), Borghei and Jabbari Sahebari (2010), Balouchi and Shafai Bejestan (2012), Nazari Giglou et al. (2016), Amini et al. (2017), Wuppukondur and Chandra (2017). There are many studies in category three which is the focus of the current study. To the best of the author's knowledge, these experimental studies are shown in Table 1.

In Table 1, flatbed refers to the conditions that velocities are measured while the bed topography is flat and there is no scouring. Flatbed without d_{50} refers to the research without using the sediment at the bottom of the flumes. In contrast with the flatbed, developed bed refers to the condition that velocities are measured above the scoured bed. Another phrase is clear water which means there is no supplying sediment or sediment feeder. On the other hand, bed load in this table refers to the condition with sediment feeder or sediment supply, and consequently, there is a bed load during the experiments.

According to Table 1 and experimental studies of flow pattern, Best and Reid (1984) evaluated the flow pattern of a small sediment-free channel confluence with the width of 0.15 m and angles of 15°, 45°, 70°, and 90°. They showed that the length and width of the separation zone at confluence increased by increasing the confluence angle and the discharge ratio. Best (1987) investigated the flow dynamics of a small sediment-free channel confluence of 0.15 m and angles of 15°, 45°, 70°, 90° and 105°. Besides showing six flow zones (Fig. 1), he evaluated the effect of flow pattern on the bed morphology of river confluences such as a formed bar, which are mentioned earlier. Ramamurthy et al. (1988) evaluated a 90° sediment-free channel confluence. They derived a relation between the depth of the flow at the confluence and the discharge ratio based on the momentum principle. Flow pattern at a 30° river confluence with bed discordance of main and tributary channels was investigated by Biron et al. (1996). They concluded that considering the bed discordance is important in river confluence modeling. Moreover, it distorted the mixing layer into the shallower channel, leading to the flow upwelling from the channel deeper into the shallower. Gurram et al. (1997) extended the knowledge about the flow pattern at the sediment-free channel confluence with angles of 30°, 60° and 90° by considering the transcritical flow conditions.

Around two decades ago, research on river confluence advanced significantly in terms of using experimental instruments and analyzing methods. Weber et al. (2001) are the pioneers who improved the knowledge and data set of the 3D flow pattern in a 90° river confluence. They measured the 3D velocities with an acoustic Doppler velocimeter (ADV) and after evaluating the data; they developed a useful 3D schematic of flow structure at river confluences. Yang et al. (2009) experimentally evaluated the separation zone variation along the water depth for a 90° river confluence. They showed that the geometry and the propensity of the separation zone represent various forms with changes along the water depth of the flume. Moreover, the discharge ratio also alters the separation zone size and shape. Liu

Table 1 Experimental studies on the flow pattern at river confluences

Research	Bed topography condition	Clear water or bed load condition	θ	d_{50} (mm)
Best and Reid (1984)	Flatbed	–	15, 45, 70, 90	–
Best (1987)	Flatbed	–	15, 45, 70, 90, 105	–
Ramamurthy et al. (1988)	Flatbed	–	90	–
Biron et al. (1996)	Flatbed	–	30	–
Gurram et al. (1997)	Flatbed	–	30, 60, 90	–
Weber et al. (2001)	Flatbed	–	90	–
Yang et al. (2009)	Flatbed	–	90	–
Liu et al. (2012)	Developed bed	Clear water	90	2–20
Leite Ribeiro et al. (2012a, b)	Developed bed	Bed load in a steep tributary channel with a constant rate	90	0.8
Coelho (2015)	Flatbed	Clear water	30, 60	–
Yuan et al. (2017)	Developed bed	Clear water	90	0.9
Wang et al. (2019)	Flatbed /developed bed of a scaled river model	Clear water	30	–
Yu et al. (2020)	Developed bed	Bed load in a tributary channel with a constant rate	30, 90	0.95
Canelas et al. (2020)	Flatbed	Clear water	70	6
Zhang and Lin (2021)	Developed bed	Clear water	90	0.95
Current study	Developed bed	Bed load with various rate	60	0.6

et al. (2012) studied flow and sediment patterns at a 90° channel confluence by developing an experimental setup. They measured 3D velocities on a developed bed with a mixed material of 2 to 20 mm, with no supplementary sediment and no live bed condition for coarse material. Leite Ribeiro et al. 2012a, b evaluated the flow and sediment patterns on a 90° river confluence with a constant supply of sediment from the tributary channel. Therefore, there was clear water condition in the main channel and bed load condition in the tributary channel, in their study. They evaluated their results for the scenario of existing bed discordance between the main and tributary channels, or in other words, they considered a steep tributary channel. Coelho (2015) assessed the inequality of water surface levels at 30° and 60° sediment-free open channel junctions by using experimental data in both subcritical and supercritical flow. Yuan et al. (2017) investigated the flow and sediment pattern of urban 90° channel confluences. They measured velocities under the developed bed and clear water conditions.

Recently, Wang et al. (2019) evaluated the stage-discharge relationship at a channel confluence and a scaled model of a river confluence in China. They showed that the water level at the main channel increased due to the tributary channel flow. Yu et al. (2020) studied the effect of the morphodynamics of 30° and 90° channel confluences on the accumulation of contaminated sediment. They measured the 3D velocities under the developed bed and clear water at the main channel. Moreover, they evaluated the effect of sediment feeding in various transverse

locations of the tributary channel. Yu et al. (2020) showed the variation of flow and sediment patterns by changing the feeding locations. Canelas et al. (2020) extended the knowledge related to flow characteristics of a 70° river confluences by two experiments with and without bed discordant under the flatbed and clear water conditions. Zhang and Lin (2021) showed the effect of drastically varying the discharge ratio on flow and sediment patterns of a 90° channel confluence. They evaluated their results on the developed bed of two different scenarios under the clear water condition.

According to the above literature review and Table 1, none of the cited experimental studies evaluated the effect of various bed load ratios over the developed bed on flow pattern at a river confluence. Therefore, the current study is designed to understand the flow pattern corresponding to the river bed behavior in case of large floods. In other words, this study aims to answer the below questions:

1) What are the effects of considering developed bed and fixed bed on the flow pattern of experimental studies at river confluences?
2) What are the effects of increasing bed load of the main channel on the flow pattern of experimental studies at river confluences?

It is expected that the morphological features downstream of the confluence have a different pattern than the ones in the condition described in other literature. Thus, this paper

describes briefly what are the different bed features and investigates the corresponding flow pattern.

This paper is organized as follows: an overview of the previous studies on river confluences. The subsequent section touches on the experimental setup and detail of test cases. Then the flow pattern is discussed in various planes (i.e., x–y and y–z planes), followed by bed shear stress, and the time–average velocity profiles. Conclusions that can be drawn from the current study are summarized in the last section.

Materials and methods

Experimental setup

The experimental setup of the present study is shown in Fig. 2. This setup was consisting of the main channel with the length of 9 m, the width of 0.25 m, and the depth of 0.60 m; and a tributary channel with the length of 3 m, the width of 0.25 m, and the depth of 0.60 m. Both stilling boxes were equipped with a system to reduce the turbulence of the incoming flow. Discharge was continuously measured by a high-accuracy electronic flow meter with an accuracy of 0.01 l/s. A moveable sediment feeder was designed and calibrated to ensure consistency of feeding into the main flume (more details can be found in Balouchi and Shafai Bejestan 2012). For measuring the velocity an electromagnetic velocity meter was used in a mesh as shown in Fig. 2. The sample rate of the velocity meter is 16 Hz and each point was measured for one minute to be sure about the accuracy of velocities. Hence, the velocity of each point was extracted by averaging about 960 series of data (velocity in 3 directions). The accuracy of the velocity meter is 0.1 cm/s. For preparing the mesh shown in Fig. 2, at the main flow direction (x), the length was divided by 5 cm steps in 13 sections named S1 to S13 which consist of upstream and downstream of the confluence. These sections were also divided into 4 fixed points which have 4, 9.5, 16.5, and 22.5 cm (line 1 to line 4, respectively) from the inner bank of the main channel (y-direction shown in Fig. 2). At the z-direction of water depth of the flume, the velocity was measured at each 1.25 cm water depth (about 2 cm needed for the height of probe of velocity meter.). It should be noted that the parameters used in the x-direction (length of the flume) are x^*, u, and u^* which are dimensionless length or length ratio (x/B), velocity in x-direction, and main velocity ratio (u/u_{max}), respectively. B is the width of the flumes and u_{max} is the maximum velocity in the main direction. Besides, the parameters used in the y-direction are y^* which is dimensionless width (y/B), and v which is the velocity in the y-direction. Parameters used in the z-direction (height of the flume) are z^* which is depth ratio (z/B), and w which is the velocity in the z-direction.

Experimental procedure

In this study, the channel bed was covered with fine sand sediment with $d_{50} = 0.6$ mm to ensure the live bed condition in the main channel. In order to avoid the initial effect of incoming flow on the stability of sediment, the flow entered the channel slowly, and simultaneously the slide gate was
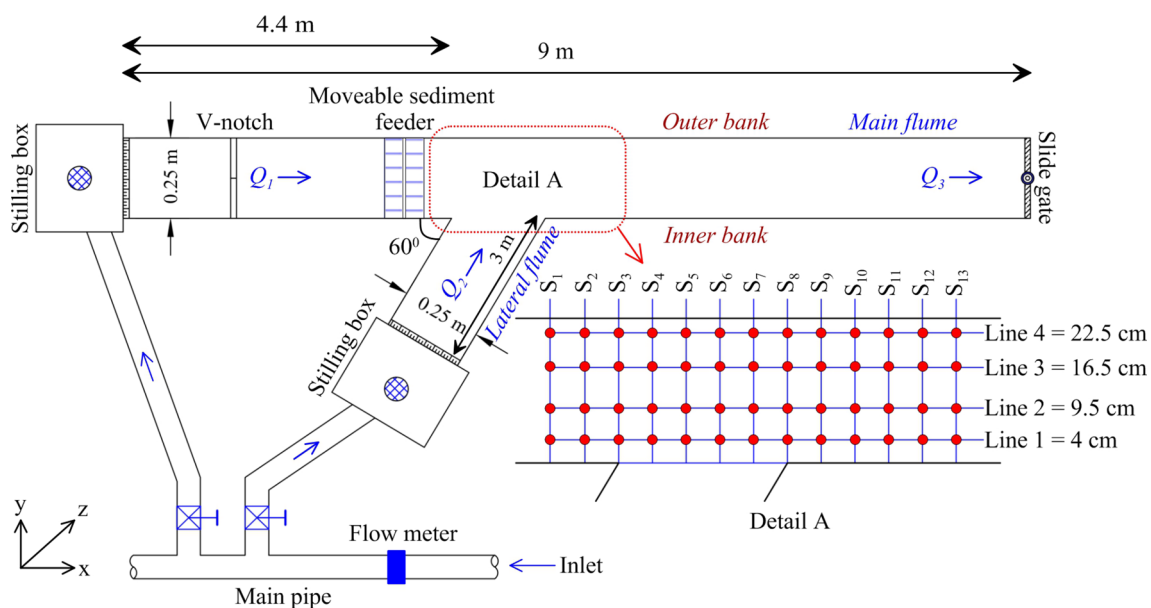

Fig. 2 Schematic view of the experimental setup

kept closed. After the flume was filled with water, the slide gate was opened gradually, and flow discharge was increased simultaneously to reach the desired water depth and discharge. These conditions were kept constant for more than an hour to reach the equilibrium condition (more details can be found in Balouchi and Shafai Bejestan 2012). Afterward, the pump was turned off and the water in the channels was extracted. Then the topography was fixed by a cement blanket method. The cement blanket method is a simple method for fixing the bed with a thin layer of cement that is covered with the same sediment size to have a constant roughness coefficient. After some hours that the cement blanket was dried, the same experiment with previous hydraulic conditions such as discharge and without sediment feeding was established, and velocities were measured at the mentioned mesh.

In the current study, two experiments with the same hydraulic conditions, but various bed load ratios (Q_b/Q_1 of 0 and 3×10^{-4}) were used. The discharge of the lateral channel (Q_2) was 4 l/s, the discharge of the main channel upstream of the confluence (Q_1) was 16 l/s, the total discharge or downstream discharge (Q_3) was 20 l/s, the discharge ratio ($Q_r = Q_2/Q_3$) was 0.2, the densimetric Froude number (Fr_g) was 6.79, d_{50} was 0.6 mm, the confluence angle was 60°, the bed slope of all channels were 0.002, water depth downstream of the confluence was 11.5 cm and the bed load ratios were 0 and 3×10^{-4}. It should be noted that the main requirement to reach goals of this study was to conduct experiments under live-bed conditions. Hence, the downstream water depth was adjusted to have the downstream densimetric Froude number of 6.79. This parameter in former studies was usually lower than 4.5 due to having clear-water conditions in the main channel.

Discussion of results

Figure 3a, b presents the developed bed under live bed condition without bedload from upstream ($Q_b/Q_1 = 0$) and with bed load ($Q_b/Q_1 = 3 \times 10^{-4}$), respectively. Q_b is the bed load from the upstream of the confluence with the same unit of discharge. It is obvious in these 2D topography contour maps that there is no point bar or deposition of sediments at the confluence (Balouchi and Shafai Bejestan 2012; Balouchi et al. 2015). Besides, the topographies or developed beds of tests with and without bed load are different. To better perceive the flow patterns at river confluence under the live bed condition and developed bed, three-dimensional flow velocity was taken by Electromagnetic velocity meter. The results of measuring velocity are discussed in the following.
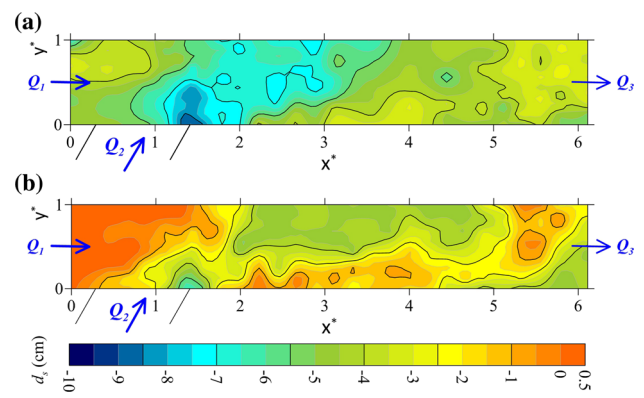

Fig. 3 Two different developed beds under live bed condition for various bed loads: **a)** $Q_b/Q_1 = 0$ and **b)** $Q_b/Q_1 = 3 \times 10^{-4}$

Main streamlines along the main channel (x–y plane)

Figure 4 shows the main streamlines along the main channel (Fig. 2: x–y plane) and the color pattern of Fig. 4 represents the dimensionless velocity (u^*) distributionin the main direction (x-direction and different planes), for a test with a discharge ratio of 0.2, densimetric Froude number of 6.79 and $\frac{Q_b}{Q_1}$ equal to zero. Figure 4a, b, c, d shows the streamlines for 2.5, 5, 7.5, and 10 cm from the water surface, respectively. It should be noted that the location of confluence (in the longitudinal axes or x*) is between 0.4 and 1.55 in Fig. 3, and the water depth at this test is 11.5 cm. Moreover, the confluence side is named the inner bank, and the opposite bank of the confluence is named the outer bank in this study.

It can be seen from Fig. 4a, b, c, d that the inflow from the lateral channel of confluence makes the approaching streamlines of the main channel deviate from the inner bank and become a curvy shape. This deviation starts with a specific deflection degree from the inner to the outer bank of the confluence. To show the deflection degree, the slope of the velocity vector can be used. For instance, the slope of the velocity vector at line 1 on the cross section S7 (lines and cross sections are shown in Fig. 2) for Fig. 4a, d is equal to 0.42 and 0.5, respectively. Thus, the deflection of streamlines toward the outer bank of the channel decreases, while moving from the water surface to the bed. In other words, this indicates that the momentum of lateral flow near the bed is less than near the water surface in the river confluence under live-bed conditions. This leads to the separation zone near the bed is narrower than the flow separation zone near the water surface. In addition, the development of the shear layer decreased by crossing the water surface to the bed due to the way of flow deflection. These results are in agreement with the
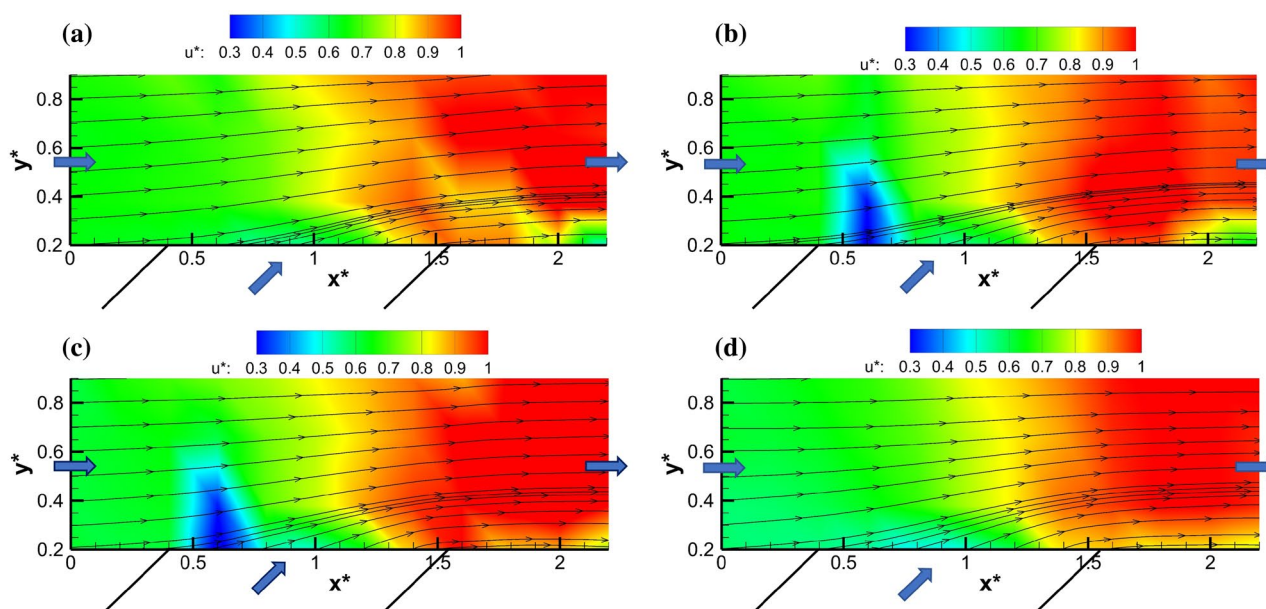
Fig. 4 Velocity contours (U^*) and flow streamlines along the main channel for: **a** 2.5, **b** 5, **c** 7.5 and **d** 10 cm from the water surface for the case of $Q_b/Q_1=0$

flow pattern of river confluence with clear water conditions (Weber et al. 2001; Yang et al. 2009; Liu et al. 2012).

One of the interesting zones in Fig. 4, is the stagnation zone. This zone is shown in blue color in Fig. 4, and generally it is also observed in this shape in the literature (Pandey and Mohapatra 2021). It can be concluded from this figure that the size of the stagnation zone varied along with the flow depth. In more detail, Table 2 represents the size of the stagnation zone for various water depths for experiments with and without bedload. It is obvious from the part without bedload of this table that the stagnation zone near the bed (with A or an equivalent area of 0.225) is more than in the surface (with A of 0.125), and it is almost maximum in the middle of the water column with an equivalent area of 0.33 and 0.36 for Fig. 4b, c, respectively. According to the results, under the live bed conditions without bedload (or clear water with high Fr_g), all the six main regions at the river confluence can be observed such as stagnation zone, flow deflection, separation zone, maximum velocity, flow recovery, and shear layers. However, at the river confluences under the live bed condition, the point bar is not existing due

to the flow and sediment hydraulics (Balouchi and Shafai Bejestan 2012; Balouchi et al. 2015), in comparison to previous studies in the literature. This result is very important for the navigation and construction of structures such as bridge piers (Ghobadian et al. 2018).

To investigate the effect of bedload and live-bed condition (which caused the different bed topographies) on flow pattern, the results of measuring velocity for a test with the hydraulic and geometric conditions like the test in Fig. 4, but $\frac{Q_b}{Q_1}$ equal to 3×10^{-4} were (Fig. 5) compared with the results of previous test case without bed load. It is obvious in Fig. 5a, b, c, d that the streamlines at the confluence deflect to the outer bank of the channel similar to Fig. 4. For comparing the deflection degree in these two tests with Q_b/Q_1 of zero and 3×10^{-4}, the slope of the velocity vector should be extracted. For instance, the slope of the velocity vector at line 1 on cross_section S7 for Fig. 5a, d is equal to 0.23 and 0.32, respectively. These results demonstrate that the flow deflection to the outer bank of the channel decreased by increasing the bedload, and the relative decrease in the

Table 2 Stagnation zone dimension for experiment with and without bedload

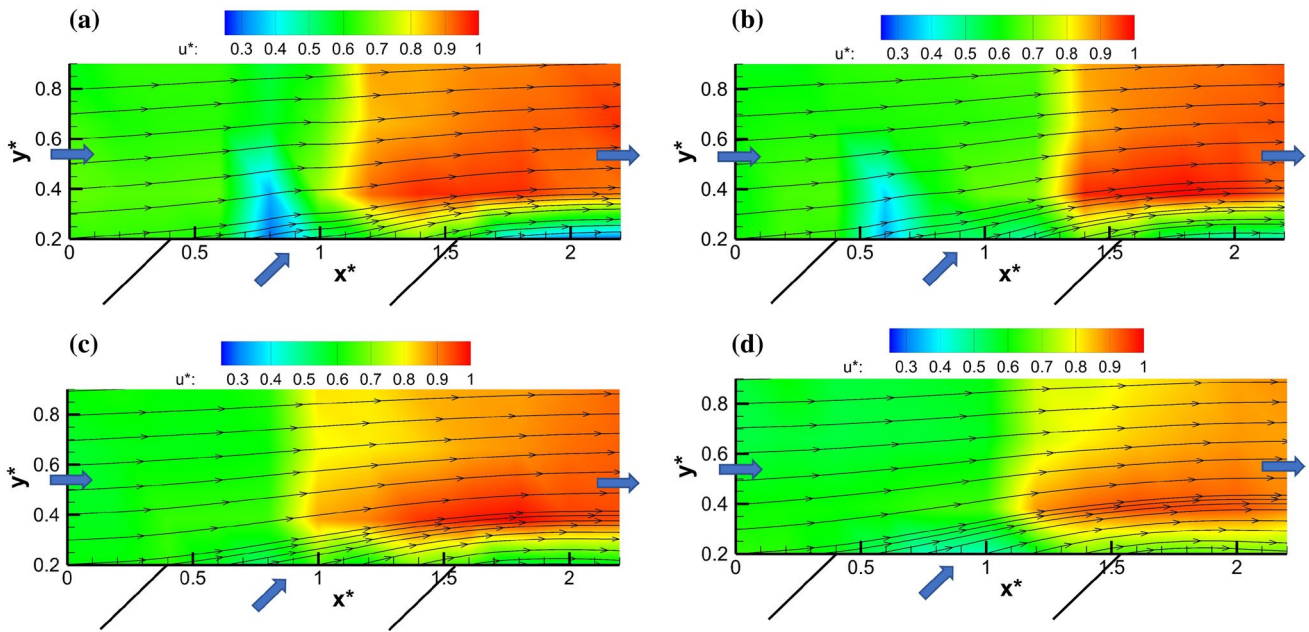| Depth from the water surface (cm)	$Q_b/Q_1=0$			$Q_b/Q_1=0.0003$		
	dx^*	dy^*	A	x^*	y^*	A
2.50	0.50	0.25	0.13	0.20	0.40	0.05
5.00	0.60	0.55	0.33	0.30	0.55	0.17
7.50	0.65	0.55	0.36	0.30	0.25	0.17
10.00	0.75	0.30	0.23	0.60	0.30	0.18

Fig. 5 Velocity contours (U^*) and flow streamlines along the main channel for: **a** 2.5, **b** 5, **c** 7.5 and **d** 10 cm from the water surface for the case of $Q_b/Q_1 = 3 \times 10^{-4}$

deflection degree is 36% for the surface and 45% for the bed. In addition, one can also conclude the momentum of lateral flow decreased by increasing the bedload. These are due to the topography formed in the channels according to the live bed condition and bedload. It should be noted that helical cells in the flow pattern of river confluences caused the scouring and variations in the bed topography (Canelas et al. 2020).

In addition, according to Fig. 5 and live bed condition, in the main channel there should be flow and sediment hydraulics in such a way that sediments move. Therefore, almost the green color in the flow pattern of Fig. 5 shows the velocity more than the critical velocity for sediment movement. Hence, according to the color of the separation zone (or velocities values) which is almost green, a lack of point bar in the river confluences with live bed conditions can be proved. In other words, it can be concluded that the mean longitudinal velocity of the separation zone is almost near to the main channel upstream of the confluence.

The results of Fig. 4 are almost similar to the results of Fig. 5. As mentioned before, the deflection degree affects the flow separation zone and stagnation zone. Thus, it can be concluded that by increasing bed load the flow separation zone, and stagnation zone decreased. Table 2 shows the stagnation zone dimensions and equivalent areas (A) for the experiment with Q_b/Q_1 of 3×10^{-4}. The trend of variation in the stagnation zone dimensions is almost the same as an experiment without bedload and it varies from the water surface to the bed with A of 0.05 to 0.18. Hence, increasing

the bed load from 0 to 3×10^{-4} can decrease the stagnation equivalent area up to 2.5 times. Moreover, according to Fig. 5, it should be noted that by increasing the bedload, the variation of the formed bed topography along the channel increased (i.e., one can see various kinds of ripples and dunes), and consequently, the variations of velocity components (u, v, w) increased. Hence, the location and magnitude of the maximum velocity zone changed downstream of the confluence. In other words, according to the formed topography in the case with bedload, the uniform flow occurred at a longer distance after the confluence compared to the case without bedload.

Transverse vectors field at the cross sections (y–z plane)

Figure 6a–d shows the transverse vectors field created at the section of confluence (y–z plane) for the longitudinal distance of 5, 20, 35 and 50 cm from the inner wall of the confluence (cross sections S4, S7, S10, and S13, respectively). All the hydraulic and sedimentary conditions are the same as the results in "Main streamlines along the main channel (x–y plane)" Section. The legend of Fig. 6 shows the dimensionless velocity (u^*) in the main direction of the channel (x-direction). It should be noted that the left side of Fig. 6a–d corresponds to the side of the channel in which the confluence exists (inner side). The flow from the tributary channel returned near the shear layer and caused a negative velocity component in the z-axis direction owing to gravity.
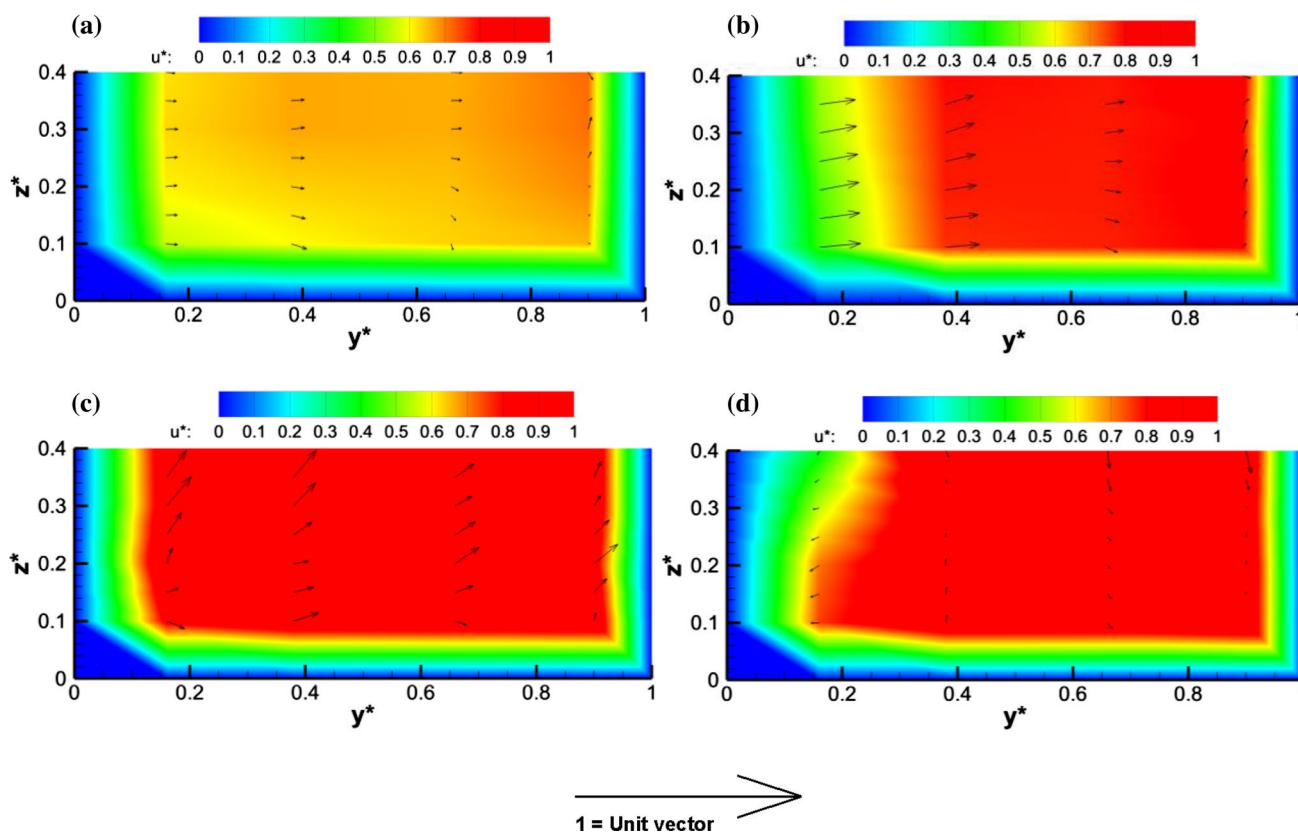
Fig. 6 Velocity contours (U^*) and transverse streamlines in the y–z plane at cross sections of: **a** S4, **b** S7, **c** S10, **d** S13, for the case of $Q_b/Q_1 = 0$

This flow characteristic resulted in an obvious secondary-flow phenomenon after the confluence. One can observe from Fig. 6, that the flow velocity across the transverse channel changes due to the presence of secondary flow, vortices, and the existence of six main zones at channel confluence. This result is also observed in the literature such as Weber et al. (2001), Yang et al. (2009), and Zhang and Lin (2021). Although secondary flow and vortices exist in Fig. 6d, it can be seen in this figure that the power or magnitude of transverse vectors is decreased, and flow is in the recovery zone. Moreover, it is obvious in this figure that the separation zone shape varies both longitudinally and transversely. It should be noted that as there is no point bar according to the hydraulic and sediment conditions of this experiment, the flow is stronger in the separation zone compared to the results in the literature without live bed condition (Weber et al. 2001).

To evaluate the effect of bedload from the main channel on the flow pattern of river confluence, another experiment was designed with $\frac{Q_b}{Q_1}$ of 3×10^{-4}. It should be noted that all the boundary conditions of the test case represent in Fig. 7 are the same as Fig. 6, except for the bed load ratio. By comparing these two figures, it can be seen that by changing the bed load or feeding sediment, the location of the maximum velocity zone is changed in almost all sections. Furthermore, the form and shape of secondary flow and vortices also are changed. These variations are due to differences in bed topography formed in the tests with different bed loads and the changes in the separation zone. In addition, in Fig. 7d (with $Q_b/Q_1 = 0$) the magnitudes of transverse vectors are still high in comparison to Fig. 6d (with $Q_b/Q_1 = 3 \times 10^{-4}$). Therefore, one can conclude from Fig. 7 that the flow recovery zone occurred at a longer distance in comparison to Fig. 6. In other words, by increasing the bed load the location of observing the recovery zone increased.

Normalized bed shear stress

The transverse distribution of normalized bed shear stress (τ_b/τ_0) of the main channel is another interesting parameter that is important in river confluences. Figure 8a–e illustrates the variation of normalized bed shear stress along dimensionless width (y^*) for S1, S5, S6, S8, S10, and S12 cross sections, respectively. It should be noted that y^* of 0 is the inner bank and 1 is the outer bank of the confluence. τ_0 is the mean bed shear stress downstream of the river confluence, and τ_b is the bed shear stress computed based on the equations below (Bahrami Yarahmadi et al. 2020):
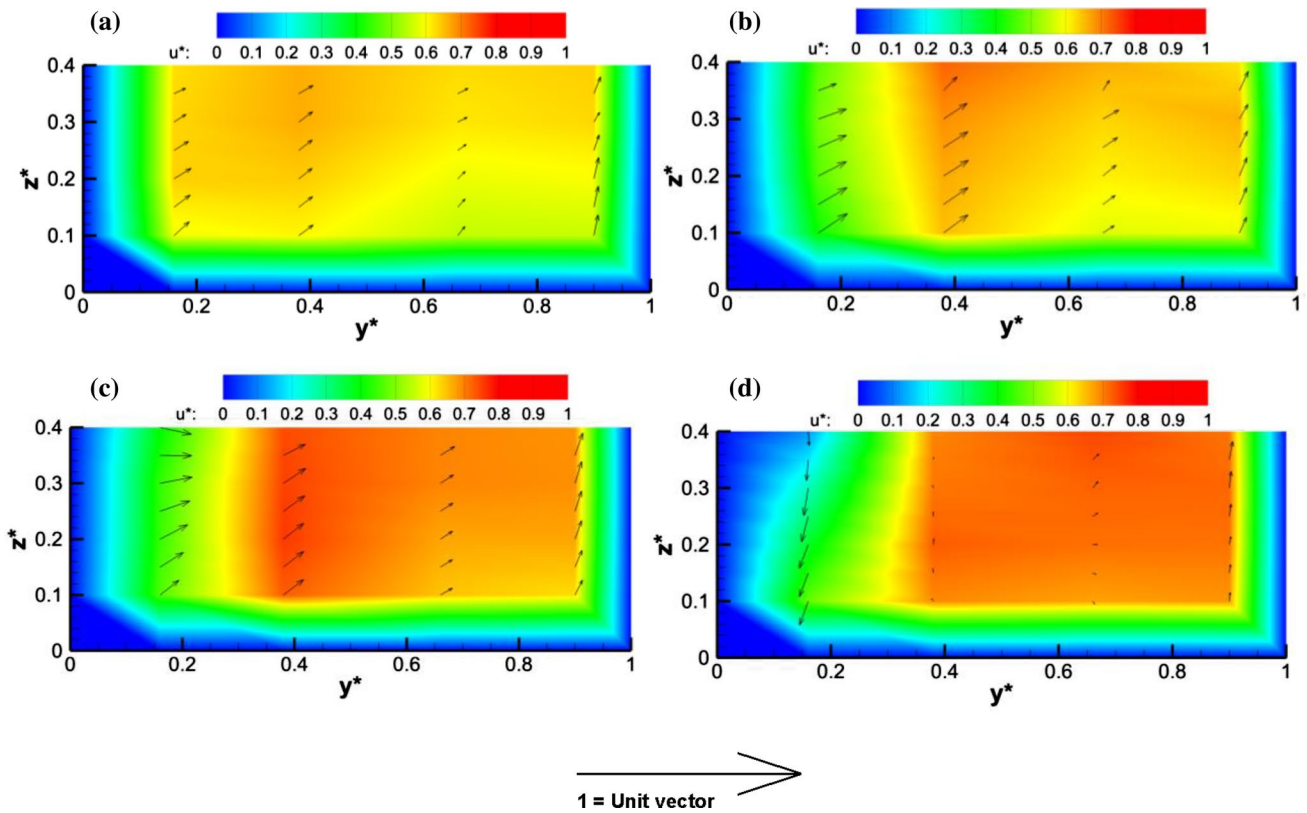
Fig. 7 Velocity contours (U^*) and transverse streamlines in the y–z plane at cross sections of: **a** S4, **b** S7, **c** S10, and **d** S13, for the case of $Q_b/Q_l = 3 \times 10^{-4}$

$$\tau_b = \sqrt{\tau_{bv}^2 + \tau_{bu}^2} \tag{1}$$

$$\tau_{bu} = \frac{\rho g}{c^2} \overline{U} \sqrt{\overline{U}^2 + \overline{V}^2} \tag{2}$$

$$\tau_{bv} = \frac{\rho g}{C^2} \overline{V} \sqrt{\overline{U}^2 + \overline{V}^2} \tag{3}$$

$$C = \frac{1}{n} R_h^{\frac{1}{6}}, \tag{4}$$

where τ_b, τ_{bu} and τ_{bv} are total bed shear stress (N/m^2) and bed shear stress in x and y directions (N/m^2), respectively. ρ is the density of fluid which is 1000 kg/m^3, g is the acceleration due to the gravity of 9.8 m/s^2, $\overline{U}$ and $\overline{V}$ are depth-averaged velocities in x and y directions (m/s), respectively. C is the Chezy coefficient, R_h is the flow hydraulic radius and n is Manning's roughness coefficient. The Depth-averaged velocities are calculated via the below equations:

$$\overline{U} = \frac{1}{h} \int_{z_b}^{z_s} U \, dz \tag{5}$$

$$\overline{V} = \frac{1}{h} \int_{z_b}^{z_s} V \, dz, \tag{6}$$

where h is the water depth (m), z_s and z_b are water and bed surface levels (m), respectively.

Figure 8a shows that bed shear stress upstream of the confluence (S1) is almost constant by changing the bed load. Then, in Fig. 8b and by starting the confluence (S5) the deviation between the normalized bed shear stress lines for with and without bedload (i.e., Q_b/Q_l of 0 and 0.0003) increased. This increase in the bed shear stress at the inner bank of the confluence ($y^* < 0.5$) is more than at the outer bank of the confluence ($y^* > 0.5$), and this is due to the momentum of lateral flow. Figure 8c shows almost the middle of the confluence (S6) and represents that the bed shear stress at the inner bank of the confluence which is almost the zone of stagnation is constant by changing the bedload, and after that, the bed shear stress increases by decreasing the bedload. After the confluence (Fig. 8d, e or S8 and S10) the maximum velocity zone is obvious at $y^* = 0.38$ and it shows that in this zone bed load is not effective on the bed shear stress. However, we have a dramatic difference at the inner bank of the confluence ($y^* = 0.16$) which is the separation zone. Besides, the maximum bed shear stress
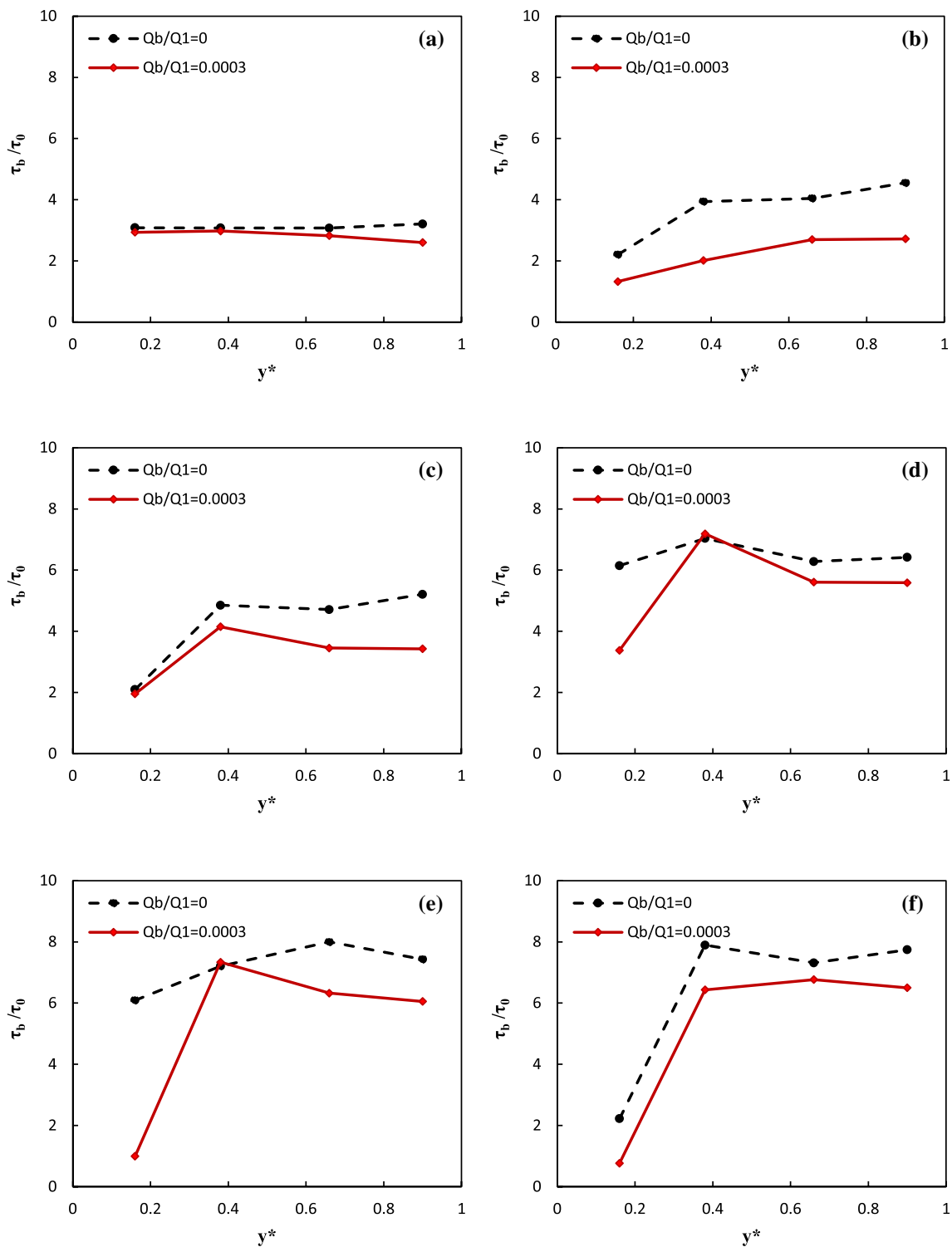
Fig. 8 Normalized bed shear stress (τ_b/τ_0) distribution along dimensionless width (y^*) for: **a** S1, **b** S5, **c** S6, **d** S8, **e** S10 and **f** S12 cross sections

after the confluence is observed around the middle of the channel which is the same observation in Roy and Bergeron (1990) study which is related to a river confluence in Canada. In addition, the trend of variation of bed shear stress in all sections has in agreement with the results of Pandey and Mohapatra (2021). It can be concluded that by increasing the bedload, the bed shear stress at the separation zone decreased significantly. Then, by increasing the distance

from the confluence, the flow is reaching the recovery zone, and the deviation between the lines of bed shear stress with and without bedload decreased again.

Generally, bed shear stress of the case with bed load is less than the case without bed load and this is due to differences in averaged velocities of these two test cases. According to the shear stress equations, this parameter has a direct relation with averaged velocities. The variation of averaged velocity for these two cases is discussed and explained in "Time average velocity profiles" Section.

Table 3 shows the maximum bed shear stress ratio ($\tau_{b\,(max)}/\tau_0$) for both with and without bedload (i.e., Q_b/Q_1 of 0 and 3×10^{-4}), and the percentage of relative changes in $\tau_{b\,(max)}/\tau_0$. It should be noted that the $\tau_{b\,(max)}/\tau_0$ is the maximum value τ_b/τ_0 in each cross section. According to this table, the maximum bed shear stress ratio increased from 2.98 to 7.89, by increasing the longitudinal distance (S1 to S12), generally. This trend of increasing bed shear stress is also observed in field studies in the literature (Roy and

Bergeron 1990). It can be concluded that increasing the bedload ratio of the main channel from 0 to 3×10^{-4} can reduce the bed shear stress up to 40% at river confluences. Table 3 also shows that the effect of bedload on bed shear stress is low before the confluence (with a change percentage of 7.12 at S1), then it increased before the middle of the flume (with a change percentage of 40.32 at S5), then it decreased till the end of the confluence (with a change percentage of −2.13 at S5), and then increased (with a change percentage of 14.28 at S12) till reach the normal flow condition.

Time average velocity profiles

Time average velocity distribution (main velocity ratio, u^*) along with the water depth ratio (z^*) at different transverse positions of the middle of the river confluence section (S6) for two sediment load ratios (0 and 3×10^{-4}) is shown in Fig. 9. The profiles were located at 4, 9.5, 16.5, and 22.5 cm from the confluence side (lines 1–4). These profiles show the effect of the mixing flow of the tributary to the main channel. It is obvious in both Fig. 9a, b that the velocity profiles in line 1 are in the flow deflection zone with lower velocity values in comparison with lines 2–4. This trend in velocity profiles is similar to the results of Wang et al. (2019). It should be noted that due to the mixing of the flow and bed topography caused by bedload (Fig. 9b), the velocity profile changes a little in comparison to the test case without bedload from the main channel. Besides, the maximum velocity profile for the case without bedload (Fig. 9a) is line 4 or located near the outer wall of confluence; like the results of the study by Liu et al. (2012). However, in the case with high values of bedload (Fig. 9b), this region has little change due to the formed bed topography. Therefore, defining the maximum velocity layer for installing the bridge piers, etc. should be considered with more caution in the confluences (Ghobadian et al. 2018).

Figure 10 indicates velocity profiles in section S12 downstream of the confluence at different sediment load ratios.

Table 3 Maximum bed shear stress ratio and relative changes for the cases with and without ($Q_b/Q_1 = 3\times10^{-4}$) bedload

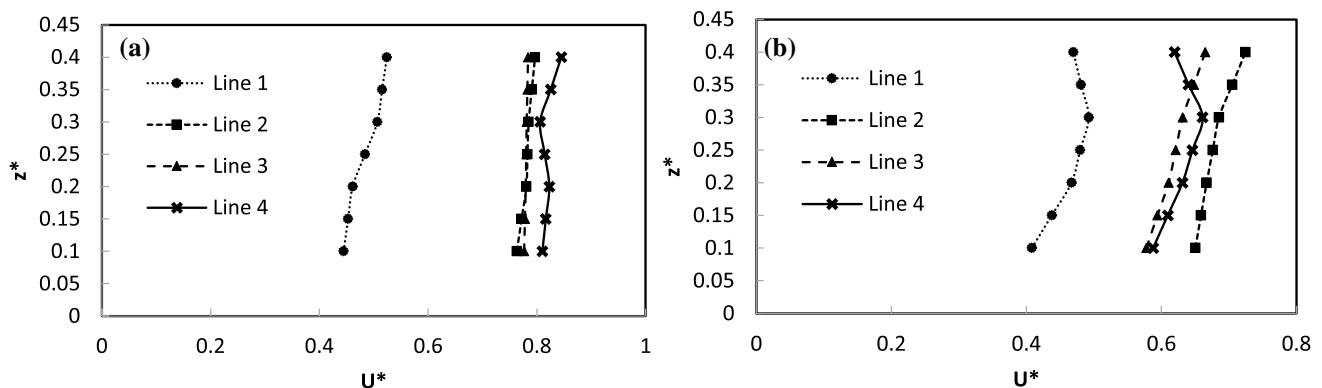| $\tau_{b\,(max)}/\tau_0$			
Cross sections	$Q_b/Q_1 = 0$	$Q_b/Q_1 = 3\times10^{-4}$	Change (%)
S1	3.21	2.98	7.12
S2	3.49	3.15	9.78
S3	3.79	3.29	13.31
S4	3.43	2.96	13.56
S5	4.55	2.72	40.32
S6	5.21	4.15	20.34
S7	6.01	5.57	7.40
S8	7.04	7.19	− 2.13
S9	7.83	7.25	7.36
S10	8.00	7.34	8.27
S11	8.10	6.79	16.11
S12	7.89	6.77	14.28

Fig. 9 Velocity profile at cross section S6 for Q_b/Q_1 of: **a** 0 and **b** 3×10^{-4}
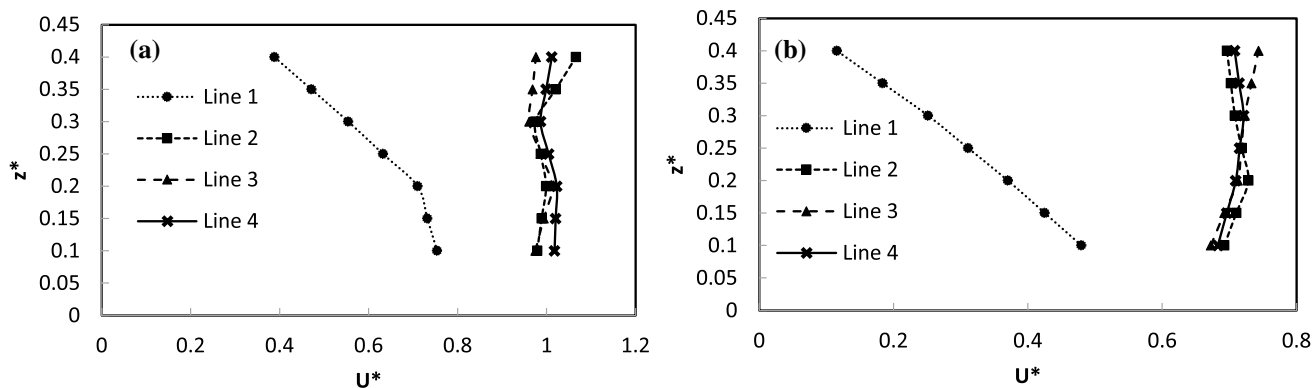
Fig. 10 Velocity profile at cross section S12 for Q_b/Q_1 of: **a** 0 and **b** 3×10^{-4}

Owing to the tributary inflow and compression flow, lines 2–4 in Fig. 10 tended to increase the velocity. For example, the mean dimensionless velocity (u^*) for lines 1–4 in Fig. 10a is equal to 0.61, 1, 0.98, and 1, respectively. In addition, these values for the case with a bedload ratio of 0.0003 are 0.3, 0.71, 0.71, and 0.71, respectively. These values and trends show that in the test case with bedload the flow needs more length to reach the flow recovery zone or uniform flow, in comparison with the case without bed load. In other words, by comparison, the values of velocities of Fig. 10a, b revealed that in the case with bedload the velocities component in the *y* and *z* directions are still stronger than in the case without bedload; and this is the reason that main velocities (in the *x*-direction) of Fig. 10a are more than 10b. This shows that the power of secondary flows increased with increasing the sediment load ratio at the confluence and the mixing flow showed a higher effect with increasing the sediment load ratio. Generally, in the entire section, the velocity became more non-uniform with increasing the sediment load ratio. Moreover, by comparing the profiles of line 1 of Fig. 10a, b it is obvious that the separation zone in Fig. 10b is more than 10a. These results are due to the change in bed topography and change in the exact location of the 3D flow structure of river confluence, which is important for navigation, river engineering, etc.

Conclusion

To the best of the author's knowledge, none of the experimental studies in the literature review evaluated the flow pattern over the developed bed with various bed load ratios at river confluences. Therefore, the current study evaluated the flow patterns of a 60° river confluence over developed beds with two-bed load ratios of 0 and 3×10^{-4} and high densimetric Froude number (6.79). The concluding remarks from the flow velocity measurement of this study are as follows:

- All the six main regions at the river confluence can be observed such as: stagnation zone, flow deflection, separation zone, maximum velocity, flow recovery, and shear layers at the river confluence affected by developed riverbed from live bed condition. However, at the river confluences under the live-bed condition, the point bar is not existing (this is also shown in Balouchi and Shafai Bejestan 2012; Balouchi et al. 2015) due to the small variation of the mean longitudinal velocity of the separation zone and the main channel upstream of the confluence. According to the literature review, most of the experimental studies about flow and sediment patterns of the river confluences mentioned that there is a point bar zone in their studies. Therefore, based on the results of the current study, this phrase should be used with more caution in future studies.

- The stagnation area of the confluence is not constant, and the maximum length of the stagnation zone can be found almost in the middle of the flow column. Moreover, increasing the bed load ratio from 0 to 3×10^{-4} can decrease the stagnation equivalent area up to 2.5 times.

- By increasing the bedload, flow deflection to the outer bank of the confluence decreased down to 36% near the water surface and 45% near the bed. Hence, the momentum of lateral flow decreased by increasing the bedload.

- In the case with bedload, the uniform flow or recovery zone occurred at a longer distance after the confluence compared to the case without bedload. Hence, the location of the maximum velocity zone changed downstream of the confluence.

- By considering variations in the bedload, the location of the maximum velocity zone, and velocity profiles along the water depth changed in almost all sections. Moreover, the form and shape of secondary flow and vortices also changed. These variations are due to differences in bed topography formed (which occurred by changing the helical cells) in the tests with different bed load ratios and the changes in the separation zone. Therefore, the maxi-

mum velocity layer for installing the bridge piers, etc., should be defined with more caution in the confluences.

- The power of secondary flows increased with increasing the sediment load ratio at the confluence and the mixing flow shows a higher effect with increasing the sediment load ratio.
- Generally, by increasing the bed load ratio from 0 to 3×10^{-4}, bed shear stress decreased at river confluence by up to 40%, and this is significantly at the separation zone.

According to the results, the flow and sediment patterns of live bed conditions have some differences from the clear water condition (such as there is no point bar). Therefore, the simultaneous effect of live bed condition and bed load from the main channel, with other effective geometric and hydraulic parameters can be considered in future studies. Besides, considering the developed bed instead of a fixed bed can reach more realistic results, in experimental works.

Conflict of interest The authors declare that they have no conflict of interests.

References

Balouchi B, Rüther N, Shafaei Bejestan M, Valerie Anne Schwarzwälder K, Bihs H (2021) 2D numerical simulation of shallow water and bedload transport in channel confluences by considering the non-hydrostatic pressure. EGU General Assembly 2021, online 19–30 Apr 2021, EGU21-9799. https://doi.org/10.5194/egusphere-egu21-9799

Ahadiyan J, Adeli A, Bahmanpouri F, Gualtieri C (2018) Numerical simulation of flow and scour in a laboratory junction. Geosciences 8:162. https://doi.org/10.3390/geosciences8050162

Amini N, Balouchi B, Shafai Bejestan M (2017) Reduction of local scour at river confluences using collar. Int J Sedim Res 32(3):364–372. https://doi.org/10.1016/j.ijsrc.2017.06.001

Bahmanpouri F, Barbetta S, Gualtieri C, Ianniruberto M, Filizola N, Termini D, Moramarco T (2022) Prediction of river discharges at confluences based on entropy theory and surface-velocity measurements. J Hydrol 606:127404. https://doi.org/10.1016/j.jhydrol.2021.127404

Bahmanpouri F, Filizola N, Ianniruberto M, Gualtieri C (2017) A new methodology for presenting hydrodynamics data from a large river confluence In: Proceedings of the 37th IAHR, World Congress, Kuala Lumpur, pp. 13–18.

Bahrami Yarahmadi M, Shafai Bejestan M, Pagliara S (2020) An experimental study on the secondary flows and bed shear stress at a 90° mild bend with and without triangular vanes. J Hydro-Environ Res 33:1–9. https://doi.org/10.1016/j.jher.2020.10.001

Balouchi B, Shafai Bejestan M (2012) The effect of bed load on maximum scour depth at river confluence. Ecol Environ Conserv 18(1):157–164

Balouchi B, Nikoo MR, Adamowski J (2015) Development of expert systems for the prediction of scour depth under live-bed conditions at river confluences: application of ANNs and the M5P model tree. Appl Soft Comput J 34:51–59. https://doi.org/10.1016/j.asoc.2015.04.040

Best JL (1987) Flow dynamics at river channel confluences: Implications for sediment transport and bed morphology. In: Frank Ethridge G, Romeo Flores M, Michael Harvey D (eds) Recent Developments in Fluvial Sedimentology. Society for Sedimentary Geology. https://doi.org/10.2110/pec.87.39.0027

Best J, Reid I (1984) Separation zone at open-channel junctions. J Hydraul Eng 110(11):1588–1594

Biron P, Best J, Roy A (1996) Effects of bed discordance on flow dynamics at open channel confluences. J Hydraul Eng 122(12):676–682. https://doi.org/10.1061/(ASCE)0733-9429(1996)122:12(676)

Borghei SM, Jabbari Sahebari A (2010) Local scour at open channel junctions. J Hydraul Res 48(4):538–542. https://doi.org/10.1080/00221686.2010.492107

Boyer C, Roy AG, Best JL (2006) Dynamics of a river channel confluence with discordant beds: flow turbulence, bed load sediment transport, and bed morphology. J Geophys Res 111(F4) https://doi.org/10.1029/2005JF000458

Bradbrook KF, Lane SN, Richards KS, Biron PM, Roy AG (2001) Role of bed discordance at asymmetrical river confluences. J Hydraul Eng 127(5):351–368. https://doi.org/10.1061/(ASCE)0733-9429(2001)127:5(351)

Canelas OB, Ferreira R, Guillén-Ludeña S, Alegria F, Cardoso A (2020) Three-dimensional flow structure at fixed 70° open-channel confluence with bed discordance. J Hydraul Res 58(3):434–446. https://doi.org/10.1080/00221686.2019.1596988

Coelho M (2015) Experimental determination of free surface levels at open channel junctions. J Hydraul Res 53(3):394–399. https://doi.org/10.1080/00221686.2015.1013513

Constantinescu G, Miyawaki S, Rhoads B, Sukhodolov A, Kirkil G (2011) Structure of turbulent flow at a river confluence with momentum and velocity ratios close to 1: insight provided by an eddy-resolving numerical simulation. Water Resour Res 47(5):W05507. https://doi.org/10.1029/2010WR010018

Constantinescu G, Miyawaki S, Rhoads B, Sukhodolov A (2012) Numerical analysis of the effect of momentum ratio on the dynamics and sediment-entrainment capacity of coherent flow structures at a stream confluence. J Geophys Res 117(F4) https://doi.org/10.1029/2012JF002452

Ghobadian R, Shafai Bejestan M (2007) Investigation of sediment patterns at river confluence. J Appl Sci 7(10):1372–1380. https://doi.org/10.3923/jas.2007.1372.1380

Ghobadian R, Basiri M, Seydi Tabar Z (2018) Interaction between channel junction and bridge pier on flow characteristics. Alex Eng J 57:2787–2795

Gualtieri C, Filizola N, de Oliveira M, Santos AM, Ianniruberto M (2018) A field study of the confluence between Negro and Solimões Rivers. Part 1: hydrodynamics and sediment transport. CR Geosci 350:31–42

Gualtieri C, Ianniruberto M, Filizola N (2019) On the mixing of rivers with a difference in density: the case of the Negro/Solimões confluence. Braz J Hydrol 578:124029

Gurram SK, Karki KS, Hager WH (1997) Subcritical junction flow. J Hydraul Eng 123(5):447. https://doi.org/10.1061/(ASCE)0733-9429(1997)123:5(447)

Leite Ribeiro M, Blanckaert K, Roy AG, Schleiss AJ (2012a) Flow and sediment dynamics in channel confluences. J Geophys Res 117(F1):62–79. https://doi.org/10.1029/2011JF002171

Leite Ribeiro M, Blanckaert K, Roy AG, Schleiss AJ (2012b) Hydro-morphological implications of local tributary widening for river rehabilitation. Water Resour Res 48(10). https://doi.org/10.1029/2011WR011296

Liu T, Chen L, Fan B (2012) Experimental study on flow pattern and sediment transportation at a 90° open-channel confluence. Int J Sedim Res 27:178–187. https://doi.org/10.1016/S1001-6279(12)60026-2

Nazari Giglou A, Jabbari A, Shakibaeinia A, Borghei SM (2016) An experimental study of sediment transport in channel confluences. Int J Sedim Res 31(1):87–96

Pandey A, Mohapatra P (2021) Reduction of the flow separation zone at combining open-channel junction by applying alternate suction and blowing. J Irrig Drain Eng 147(10):06021011. https://doi.org/10.1061/(ASCE)IR.1943-4774.0001611

Ramamurthy A, Carballada L, Tran DM (1988) Combining open channel flow at right angled junctions. J Hydraul Eng 114(12):1449. https://doi.org/10.1061/(ASCE)0733-9429(1988)114:12(1449)

Roy A, Bergeron N (1990) Flow and particle paths at a natural river confluence with coarse bed material. Geomorphology 3(2):99–112

Shakibainia A, Majdzadeh MR, Tabatabai ZAR (2010) Three-dimensional numerical study of flow structure in channel confluences. Can J Civ Eng 37(5):772–781. https://doi.org/10.1139/L10-016

Wang X, Yan X, Duan H, Liu X, Huang E (2019) Experimental study on the influence of river flow confluences on the open channel stage–discharge relationship. Hydrol Sci J 64(16):2025–2039. https://doi.org/10.1080/02626667.2019.1661415

Weber LJ, Schumate ED, Mawer N (2001) Experiments on flow at a 90° open channel junction. J Hydraul Eng 127(5):340–350. https://doi.org/10.1061/(ASCE)0733-9429(2001)127:5(340)

Wuppukondur A, Chandra V (2017) Methods to control bed erosion at 90° river confluence: an experimental study. Int J River Basin Manag 15(3):297–307. https://doi.org/10.1080/15715124.2017.1307846

Yang QY, Wang XY, Lu WZ, Wang XK (2009) Experimental study on characteristics of separation zone in confluence zones in rivers. J Hydrol Eng 14(2):166–171. https://doi.org/10.1061/ASCE1084-0699(2009)14:2(166)

Yu Q, Yuan S, Rennie CD (2020) Experiments on the morphodynamics of open channel confluences: Implications for the accumulation of contaminated sediments. J Geophys Res Earth Surf 125(9):e2019JF00543810 https://doi.org/10.1029/2019JF005438

Yuan S, Tang H, Xiao Y, Qiu X, Xia Y (2017) Water flow and sediment transport at open-channel confluences: an experimental study. J Hydraul Res 56(3):333–350. https://doi.org/10.1080/00221686.2017.1354932

Zhang Z, Lin Y (2021) An experimental study on the influence of drastically varying discharge ratios on bed topography and flow structure at urban channel confluences. Water 13(9):1147. https://doi.org/10.3390/w13091147